catalysts

MDPI

Article

Six Flux Model for the Central Lamp Reactor Applied to an External Four-Lamp Reactor

Fernando J. Beltrán *, Javier Rivas and Juan-Fernando Garcia-Araya

Departamento de Ingeniería Química y Química Física, Instituto Universitario de Investigación del Agua, Cambio Climático y Sostenibilidad (IACYS), Universidad de Extremadura, 06006 Badajoz, Spain; fjrivas@unex.es (F.J.R.); jfgarcia@unex.es (J.F.G.-A.)

* Correspondence: fbeltran@unex.es; Tel.: +34-924-289387

Abstract: One of the difficulties of establishing the intrinsic kinetics of photocatalytic oxidation processes is due to the complex mathematical formula used to determine the rate of photon absorption. To solve this problem, some models have been proposed and checked, such as the Six Flux Model (SFM) confirmed in central lamp photoreactors. External lamp photoreactors are also one of the most used configurations to study the photocatalytic oxidation of contaminants in water, and complex mathematical solutions have been reported to solve the rate of photon absorption. In this work, SFM Equations already reported for the central lamp photoreactor have been adapted to determine the rate of photon absorption in an external four-lamp photoreactor. The results obtained show slight differences from those of the Monte Carlo method. Additionally, once the rate of photon absorption was validated, the intrinsic rate constant and scavenging factor of the photocatalytic oxidation of some contaminant compounds from results already published have been determined.

Keywords: volumetric rate of photon absorption; six flux model; external lamp photoreactor; photocatalytic oxidation kinetics; scavenging factor; water organic contaminants

Citation: Beltrán, F.J.; Rivas, J.; Garcia-Araya, J.-F. Six Flux Model for the Central Lamp Reactor Applied to an External Four-Lamp Reactor. *Catalysts* **2021**, *11*, 1190. https://doi.org/10.3390/catal11101190

Academic Editor: Roberto Fiorenza

Received: 15 September 2021
Accepted: 28 September 2021
Published: 29 September 2021

1. Introduction

It is well known that Advanced Oxidation Processes (AOPs), are the only technologies capable of destroying water contaminants at ambient conditions due to the high oxidizing power of hydroxyl radicals generated in these processes [1,2]. Photocatalytic oxidation (PCO) of water contaminants with ozonation and Fenton oxidation are some of the advanced oxidation processes that have attracted a lot of research interest in the last two decades [3–7]. In this century, literature shows more than 6700 papers on this subject; a figure similar to that of ozonation or Fenton processes, with about 7100 and 5500 papers, respectively, according to the Scope database. PCO consists of the irradiation of semiconductor material to produce positive (holes) and negative (electrons) charges when the energy of radiation at least equals the band gap energy of the semiconductor [8]. Strong oxidant holes and reducing electrons then migrate from the valence and conduction bands, respectively, to the surface of the catalyst to directly, in the case of holes, or indirectly, through species formed from them (hydroxyl, superoxide radicals, etc.), react with the organics present in water [9]. It is evident that absorption of energy is the key step of PCO. The knowledge of the rate of photon absorption is fundamental to establishing the contaminant oxidation rate. The main variables affecting the photon absorption rate concern the geometry of the reacting system (photoreactor), the intensity of radiation and the optical properties of the catalyst, among others [10,11]. When solving the photocatalytic oxidation rate of any contaminant, the radiation transfer equation and the mass balance of the target compound and, in some cases, fluidodynamic aspects are needed, with the former as the most difficult step to be solved [12]. Literature has already reported complicated mathematical models to solve the radiation transfer equation or algorithms based on Monte Carlo methods that cannot be easily applied to any geometry of a given

photoreactor [13–15]. This is because these methods and models have to consider the possibilities that one photon can be absorbed, transmitted or dispersed when it reaches a catalyst particle in the reacting medium. More recently, methods based on the probability that one photon can be dispersed after its collision with the catalyst particle by following different directions have also been proposed [16,17]. Among these models, the so-called Six Flux Model (SFM), which is based on the six cartesian directions that the photon can follow after any collision, has been checked and confirmed in a cylindrical photoreactor with a central located UV lamp (central lamp photoreactor). This configuration is likely the preferred option to study the PCO of water contaminants [18,19]. In this photochemical reactor, radiation coming from the central axis, where the lamp is placed, radially travels to reach the reaction media limited between two cylinders. SFM perfectly calculates the local volumetric photon absorption rate (LVRPA) as a function of the axial and radial coordinates. Next, considering the knowledge of the optical catalyst properties, reactor dimensions and the probability function that any photon has to follow the six cartesian directions after colliding with a catalyst particle, the overall absorption rate of photon absorption (OVRPA) of the catalyst can also be calculated. In addition to central lamp photoreactors, external n-lamp photoreactors have also been used in PCO, and their OVRPA was solved by means of Monte Carlo methods [20–22].

Given the similar geometry and radial transport of radiation of the external lamp and central lamp photoreactors, an attempt to apply the SFM equations established for the latter to the former constitutes the first objective of this work. Additionally, a second objective was to determine the rate constant of the reaction of some organics in PCO once the OVRPA has been determined, that is, the intrinsic kinetics of PCO.

2. Results and Discussion

Figures 1 and 2 show the typical schemes of the central lamp and four external lamps photoreactors with their corresponding axial and radial dimension variables, among others.

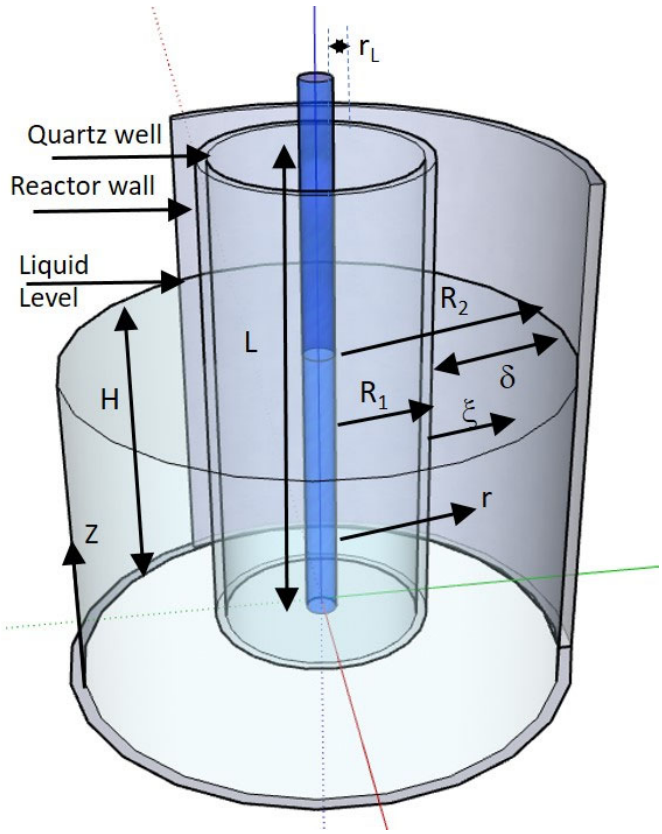

Figure 1. Scheme of the central lamp photoreactor and principal dimensions.

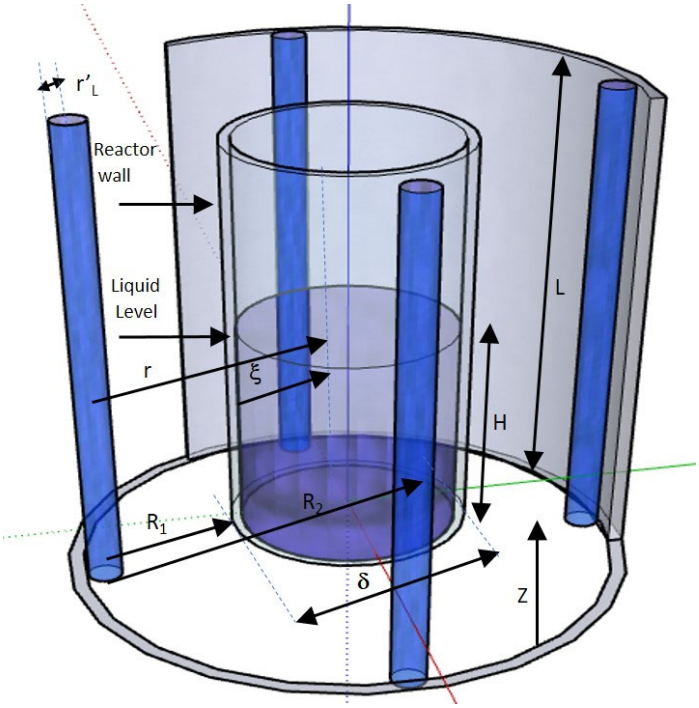

Figure 2. Scheme of the external four lamps photoreactor and principal dimensions.

For the central lamp photoreactor, the SFM yields Equation (1) to determine the local volumetric rate of photon absorption [1]:

$$\mathrm{LVRPA} = \mathrm{K}f(z^*)f(\xi^*) \tag{1}$$

with K, f(z*) and f(ξ*) defined as follows:

$$\mathrm{K} = \frac{r_L I_W \tau(1-\omega)}{2\delta\omega_{cor}} f(\omega,\tau) \tag{2}$$

where r_L is the lamp radius, I_W the incident radiation at the internal wall of the photoreactor or at the radius (R_1) of the well where the lamp is immersed, δ the length path of radiation reaction space or $R_2 - R_1$, τ, the optical density of the catalyst, ω_{cor}, the corrected albedo and f(ω,τ) a function of the scattering albedo (ω) and optical density of the catalyst (see definitions in the Supplementary section),

$$f(z^*) = \arctan\left(\frac{\beta}{2}(2\alpha z^* - \alpha + 1)\right) - \arctan\left(\frac{\beta}{2}(2\alpha z^* - \alpha - 1)\right) \tag{3}$$

where α and β are dimensionless geometrical parameters:

$$\alpha = \frac{H}{L} \tag{4}$$

$$\beta = \frac{L}{R_1} \tag{5}$$

L and H being the length of the lamp and height of the water in the reactor, respectively, and the dimensionless radial, ξ*, and axial, z*, coordinates are defined as follows:

$$\xi^* = \frac{r - R_1}{\delta} \tag{6}$$

$$z^* = \frac{z}{H} \tag{7}$$

where $r - R_1$ and z are the dimension radial and axial coordinates, respectively (see Figure 1),

$$f(\xi^*) = \frac{\exp(-\tau_{ap}\xi^*)}{R_1 + \delta\xi^*} \quad (8)$$

where τ_{ap} is the apparent optical density of the catalyst. Note that ξ^*, the dimensionless radial variable, only just covers the length of the reaction space between R_1 and R_2, that is, δ.

In order to validate SFM Equation (1) for the external four-lamp photoreactor, two assumptions have been considered:

1. Dimension variables of the central lamp photoreactor are substituted by the corresponding variables of the same symbol or name of the external lamp photoreactor so that Figure 2 becomes Figure 1. For instance, the radius of the internal wall of the assumed photoreactor was R_1, that is, the distance between the lamp and the wall of the actual external lamp photoreactor.

2. The radius of the lamp considered in Equation (1) was the diameter of the radius of any lamp of the external lamp photoreactor since it is assumed that only one lamp situated in the central axis of the photoreactor substitutes, as a radiation source, the four lamps of the actual photoreactor.

2.1. LVRPA and OVRPA

To confirm the validity of the SFM model, the external four-lamp photoreactor of reference [21] with corresponding dimensions (see Table S1 and Figure 1) was considered. In reference [21], the photocatalytic oxidation of dichloroacetic acid (DCA) with a catalyst suspension of P25 TiO_2 was studied. In the work, the authors determined the LVRPA and OVRPA by applying the Monte Carlo method, which apparently led to what can be assumed was the exact solution. In the present work, parameter values of SFM related to the optical properties of the catalyst (P25 TiO_2) have also been taken from the literature and are shown in Table S1.

As an example, LVRPA at the central lamp position ($z^* = 0.5$) as a function of the dimensionless radial variable within the reaction space ξ^* and for different catalyst concentrations has been calculated using Equations (1) to (8). Figure 3 shows, as an example, how LVRPA changes with ξ^* for concentrations between 10^{-3} and 5×10^{-2} gL^{-1} (see Figure S1 in the Supplementary information for results at other catalyst concentrations). These results show a high similarity to those previously reported [21]. As can be seen from Figure 3, for a given value of ξ^* close to the reactor wall ($0 < \xi^* < 0.1$), the higher the catalyst concentration, the higher the LVRPA. However, at higher ξ^* values, the opposite situation is observed, though in these cases, LVRPA presents extremely low values or even negligible. This is the result of the increasing scattering radiation as the concentration of catalyst increases. At high catalyst concentrations, the absorption of photons is high as far as they collide with external catalyst particles situated close to the photoreactor's wall, where radiation arrives. Nevertheless, at higher ξ^* values, a low amount of photons reached this reaction media location. As a consequence, absorption rates' negligibility significantly diminished, especially for high catalyst concentration (see Figure S1).

The next step was the determination of OVRPA from the integration of LVRPA into the reaction volume as follows:

$$OVRPA = \int_0^V LVRPA\ dV = \int_{R_1}^{R_2}\int_0^H LVRPA\ 2\pi r dr dz = 2\pi H\delta \int_0^1\int_0^1 (R_1 + \delta\xi^*)LVRPA\ \ dz^* d\xi^* \quad (9)$$

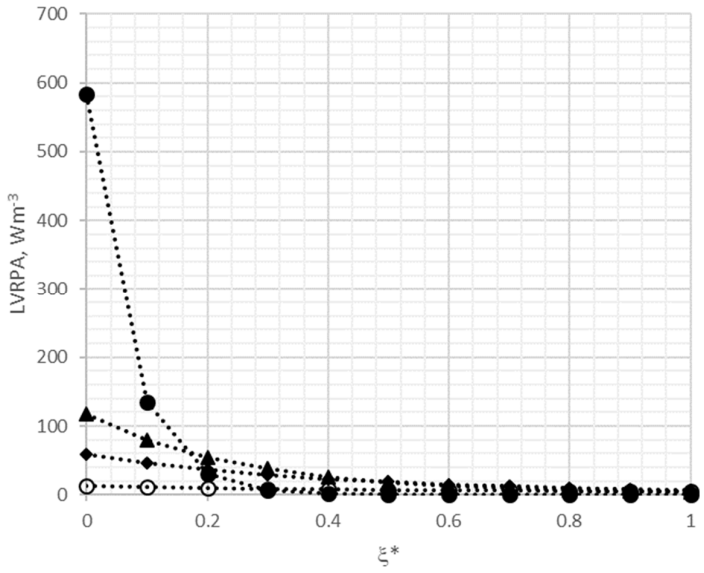

Figure 3. Local Volumetric Rate of Photon Absorption (VRPA) vs. ξ* from Six Flux Model (SFM) adapted to the external four-lamp photoreactor. Variation with dimensionless radial position within the reaction space and catalyst concentration. Catalyst concentration, gL^{-1}: ○ 10^{-3}, ♦ 5×10^{-3}, ▲ 10^{-2}, ● 5×10^{-2}.

Figure 4 shows the values of OVRPA deduced for different catalyst concentrations.

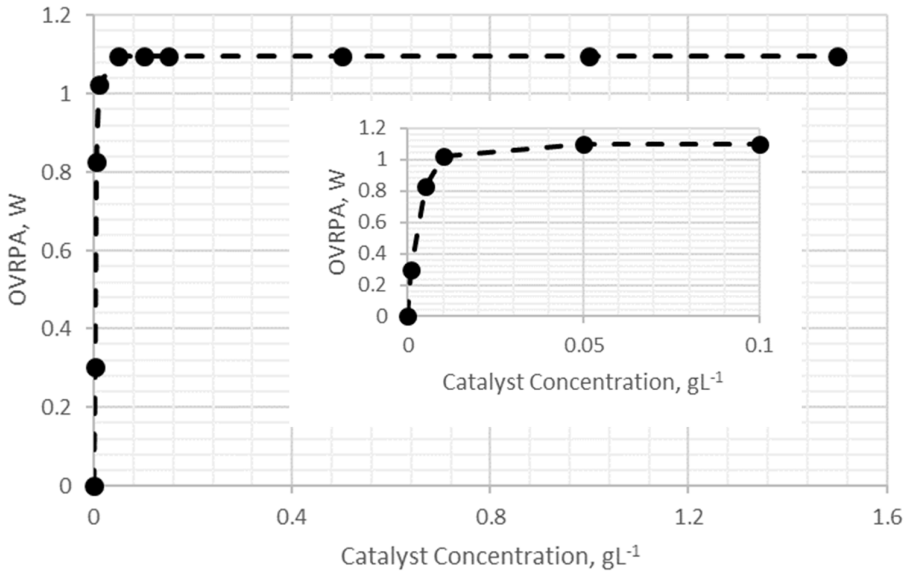

Figure 4. Variation of Overall Volumetric Rate of Photon Absorption (OVRPA) with catalyst concentration.

As can be seen from Figure 4, the increase in the catalyst concentration up to about 0.05 gL^{-1} leads to another corresponding increase in the OVRPA. Catalyst concentrations above this value resulted in a constant value of the OVRPA. This is an expected trend due to the increasing radiation dispersion that the catalyst provokes when its concentration is high. In Figure 5, a comparison of the results obtained with SFM in this work and the Monte Carlo method of Rivas et al. [21] in terms of percentage of absorbed radiation at different catalyst concentrations is shown. As observed from Figure 5, the application of SFM corresponding to the internal lamp photoreactor predicts with deviations lower than 10% the results from the Monte Carlo method for concentrations higher than 0.05 gL^{-1} of catalyst, while it overestimates the results from the Monte Carlo method at low concentrations. In any case,

research commonly works on photocatalytic oxidation are carried out above the limit of catalyst concentration, that is, at concentrations leading to the highest photon absorption rate. In this sense, the application of SFM to the external lamp reactor as if it would behave as a central lamp photoreactor can be a good option to know the overall volumetric rate of photon absorption.

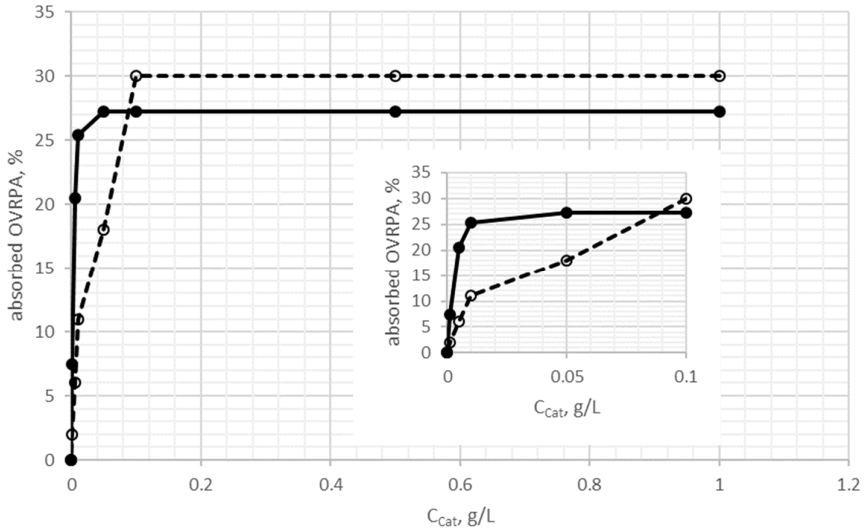

Figure 5. Percentage of absorbed radiation with catalyst concentration from the SFM model (●) and the Monte Carlo method (percentages values from these method deduced from [21] (○).

2.2. Kinetics of Photocatalytic Oxidation of Some Organic Contaminants

The photocatalytic oxidation rate of contaminants in water usually follows Langmuir kinetics [23,24], which, in many cases, reduces to first-order kinetics when the product of the equilibrium adsorption constant and the concentration of the contaminant is significantly lower than 1. This is the normal scenario in real cases of water treatment where the concentration of the contaminant is low [25]:

$$-r_M = \frac{k_M C_M}{1 + K_M C_M} \simeq k_M C_M \text{ if } K_M C_M << 1 \quad (10)$$

This first-order kinetics, however, can also be confirmed by considering that hydroxyl radical oxidation is the main way to remove contaminants when photocatalytic oxidation is applied. This way of reaction can be produced if hydroxyl radicals are formed from the positive holes in the valence band of the semiconductor:

$$h^+ + H_2O_{ads} (\text{or } -OH_{ads}) \rightarrow HO\bullet \quad (11)$$

and even from successive steps starting with the formation of superoxide ion radicals in the conduction band of the semiconductor:

$$e^- + O_2 \rightarrow O_2^-\bullet \rightarrow \ldots H_2O_2 \rightarrow \ldots HO\bullet \quad (12)$$

Both ways of reaction have been extensively reported in photocatalytic oxidation works [26]. With this assumption and provided that a contaminant M does not directly photodecompose, its photocatalytic oxidation rate would be:

$$-r_M = k_{HOM} C_{HO} C_M \quad (13)$$

where k_{HOM} is the rate constant of the reaction between hydroxyl radicals and M; and the concentration of these free radicals, C_{HO}, is the ratio between their initiation rate, r_{in}, and the sum of the products between the concentration of any hydroxyl radical scavenger

substance, C_{Si}, and the corresponding rate constant of its reaction with hydroxyl radicals, $k_{HOSi.}$ This term is usually called the scavenging factor, SF [27]:

$$C_{HO} = \frac{r_{in}}{\sum k_{HOS_i} C_{S_i}} \quad (14)$$

In Equation (14), the initiation rate of radicals is the product between the catalyst quantum yield, ϕ_{cat}, and OVRPA, so that Equation (13) becomes Equation (15), that is, first-order kinetics as in Equation (10):

$$-r_M = k_{HOM} \frac{\phi_{cat} OVRPA}{\sum k_{HOS_i} C_{S_i}} C_M = k_M C_M \quad (15)$$

It should be noted that the SF can change with reaction time because of the changing nature of byproducts formed over time that are usually of increasing hydroxyl radical scavenging character [28].

Determination of the Intrinsic Rate Constant of Photocatalytic Oxidation

According to Equation (15), the ratio between the rate constant k_{HOM} and SF, that is, the intrinsic rate constant of photocatalytic oxidation, can be obtained from k_M once the quantum yield of the catalyst and the OVRPA are known:

$$\frac{k_{HOM}}{\sum k_{HOS_i} C_{S_i}} = \frac{k_M}{\phi_{cat} OVRPA} \quad (16)$$

Notice that this intrinsic rate constant depends on the nature of the aqueous medium since scavenger concentrations affect the oxidation rate of a given contaminant M. In this work, the intrinsic rate constant of a series of contaminants has been determined in ultrapure water. Data on the photocatalytic oxidation of these compounds have been taken from previous works by this research group [20–22]. Table 1 shows the lists of compounds, their k_{HOM} values and the works where the results are published.

Table 1. Contaminants considered and their corresponding hydroxyl radical rate constant values.

Compound	Reference for Results	$k_{HOM} \times 10^{-9}$, $M^{-1}s^{-1}$	Reference for k_{HOM}
Dichloroacetic acid, DCA	[21]	3.9	[29]
2-methyl-4-chlorophenoxyacetic acid MCPA	[20]	6.6	[30]
Metoprolol (MTP)	[22]	7.3	[31]
Diclofenac (DCF)	[22]	7.5	[32]
Ketorolac (KTR)	[22]	7.3	[31]

In these quoted works, an increase of 4 °C in one hour was observed in the reaction medium due to the radiation applied. At first, this can affect the process kinetics. However, in photocatalytic oxidation, the rate constant k_M in Equation (10) depends on the catalyst quantum yield, radiation intensity applied and rate constants of reactions involving free radical and charged species, such as electrons and holes (see Equations (11) and (12)). These parameters, in fact, hardly have a significant influence on photocatalytic kinetics. For instance, Chen et al. [33] carried out photocatalytic runs for the removal of methylene blue, MB, in the 20 to 70 °C temperature interval with minimal differences in MB conversion with time. Accordingly, the temperature effect was neglected in the kinetic study of this work.

Additionally, literature reports negligible adsorption on TiO_2 of Dichloroacetic acid (DCA), Metoprolol (MTP), Ketorolac (KTR) and Diclofenac (DCF) [12,22]. Then, for these compounds, the simplification of Langmuir kinetics to a pseudo-first-order one can be conducted. With respect to 2-methyl-4-chlorophenoxyacetic acid (MCPA), Zertal et al. [34] reported less than 20% adsorption on TiO_2, and taking into account the number of vacant sites of the catalyst [35], a value of the adsorption equilibrium constant K_M = 6303.3 M^{-1} is found, as shown in the Supplementary section. Then, the product $K_M C_M$ at the start of

oxidation (see Equation (10)) is 1.57, which is higher than 1. Therefore, Langmuir kinetics cannot be reduced to simple pseudo-first-order kinetics. However, the relationship between k_M and parameters of Equation (15) still hold, that is:

$$k_M = k_{HOM} \frac{\phi_{cat} OVRPA}{\sum k_{HOS_i} C_{S_i}} \quad (17)$$

In Equation (17), the quantum yield of the catalyst, P25 TiO_2, (ϕ_{Cat}) for the concentrations used in the quoted works [20–22], between 0.15 and 0.5 gL^{-1}, and the radiation source emitting between 350 and 410 nm were taken as 3.7×10^{-3} $molEinstein^{-1}$ from Tolosana-Moranchel et al. [36]. Incident radiation at the reactor wall ($r = R_1$) was 1.19×10^{-5}, 1.15×10^{-6} and 8.33×10^{-7} $EinsteinL^{-1}s^{-1}$ for the works from [20–22], respectively.

From the above conclusions, the kinetics of the photocatalytic oxidation of compounds in Table 1 follows the Langmuir model for MCPA and pseudo-first-order for the rest of the compounds. In any case, the external four-lamp photoreactors of quoted references worked as semicontinuous (oxygen was continuously provided) perfectly mixed tanks, so that the mass balance of any compound in these reactors during photocatalytic oxidation is given by Equation (18):

$$\frac{dC_M}{dt} = r_M \quad (18)$$

- Case of first-order kinetics

Solving differential Equation (18) with $r_M = -k_M C_M$ yields the concentration profile of M with time:

$$C_M = C_{M0} \exp(-k_M t) \quad (19)$$

Equation (19) for the photoxidation of the compounds shown in Table 1, which follow first-order kinetics, was confirmed in all cases though it depended on the reaction time (see Figure 6 for the case of DCA at different concentrations as an example).

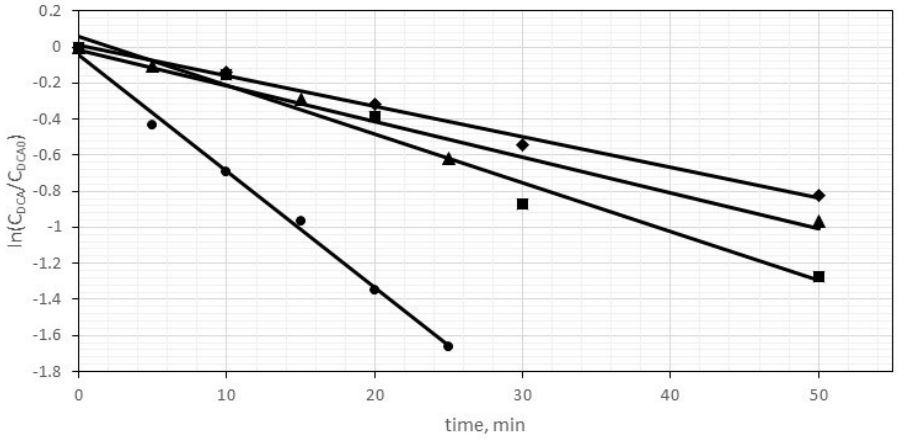

Figure 6. First-order kinetics for the photocatalytic oxidation of Dichloroacetic acid (DCA) (experimental data deduced from [21]). Initial DCA concentration, mgL^{-1}: ● 5; ■ 20; ▲ 50; ♦ 70.

This means that the higher the initial concentration of contaminant, the higher the reaction time where first-order kinetics applies. For instance, for the case of pharmaceuticals MTP, DCF and KTR, the results from [22] for 20 and 0.05 mgL^{-1} initial concentrations show that the first-order kinetics hold during the first 60 and 15 min, respectively. (In the Supplementary section, the confirmation of Equation (18) for MTP, DCF and KTR is also shown in Figure S2.) However, as pointed out before, at higher reaction times, it is likely that first order kinetics still hold but with lower rate constant values due to the increase in SF [28]. In this work, only concentration-time data corresponding to this first period of reaction was considered to determine the intrinsic rate constant.

- Case of Langmuir kinetics

  For the case of MCPA, following Langmuir kinetics, the mass balance of Equation (20) applies:

$$\frac{dC_M}{dt} = r_M = -\frac{k_M C_M}{1 + K_M C_M} \quad (20)$$

The separation of variables and integration leads to:

$$\ln\left(\frac{C_M}{C_{M0}}\right) + K_M(C_M - C_{M0}) = Y = -k_M t \quad (21)$$

Figure 7 confirms Equation (21) for photocatalytic oxidation of MCPA, where the slope of the straight line after least squares fitting, as in Figure 6, also corresponds to $-k_M$. It should be highlighted that values of k_M for MCPA photocatalytic oxidation following both the Langmuir model and first-order kinetics are nearly coincident (0.1116 and 0.104 min^{-1}, respectively). In the Supplementary section, the confirmation of Equation (19) of first-order kinetics for the case of MCPA is also presented. Accordingly, for MCPA, in spite of the non-negligible contribution of adsorption, first-order kinetics could be assumed as well.

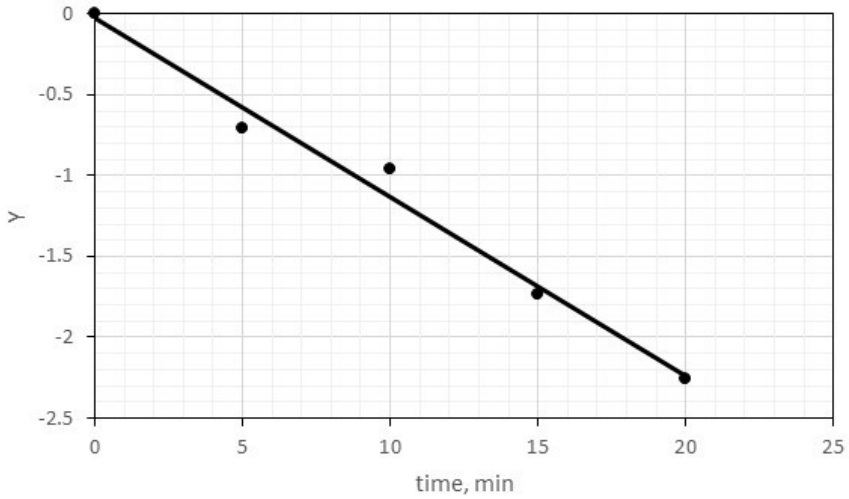

Figure 7. Langmuir kinetics for the photocatalytic oxidation of 2-methyl-4-chlorophenoxyacetic acid (MCPA) (experimental data deduced from [20]).

The values of k_M and the duration of this first initial period (for DCA, MTP, DCF and KTR) where they hold together to the one of MCPA photocatalytic oxidation are given in Table 2. From Table 2, it can be seen that for a given compound, the higher its concentration in water, the lower the intrinsic rate constant and the higher the SF. This is observed in the results of DCA and pharmaceuticals, and it is due to the lesser byproducts formed when the initial concentration was lower.

The complexity of the molecular structure of the compound also has a positive effect on SF as a result of the higher number of intermediates that can be formed from a compound of a more complex structure. This can be seen by comparing the results of DCA and pharmaceuticals at a 20 ppm initial concentration, though the difference in SF is low, 1.04×10^5 against 1.15×10^5 (mean value) s^{-1}, respectively. However, another variable that affects SF is the absorbed radiation, which was 3.24×10^{-6} and 2.27×10^{-7} $EinsteinL^{-1}s^{-1}$ for DCA and pharmaceutical photooxidation, respectively. These values are the reason for the low SF differences in spite of the more complex structure of pharmaceuticals compared to DCA. Additionally, it can be observed that SF values obtained from the simultaneous photooxidation of the three pharmaceutical compounds were similar regardless of their initial concentration. This is an expected result since, in these cases, the formed scavengers belong to the same experiment because the pharmaceuticals were simultaneously treated.

Table 2. Compounds considered, initial concentration, reaction time of first-order kinetics, first-order rate constant, intrinsic rate constant and scavenging factor.

Compound	C_{M0}, mgL^{-1}	Reaction Time, min	k^d, min^{-1}	k_{HOM}/SF [d], M^{-1}	SF^d, s^{-1}
DCA [a]	5	25	6.47×10^{-2}	9.00×10^{4}	4.33×10^{4}
	20	50	2.70×10^{-2}	3.76×10^{4}	1.04×10^{5}
	50	50	1.98×10^{-2}	2.76×10^{4}	1.42×10^{5}
	70	50	1.69×10^{-2}	2.35×10^{4}	1.66×10^{5}
MCPA [b]	5	20	1.116×10^{-1}	1.29×10^{6}	5.13×10^{3}
KTR [c]	0.05	15	5.47×10^{-2}	1.10×10^{6}	6.67×10^{3}
	20	60	3.3×10^{-3}	6.61×10^{4}	1.10×10^{5}
DCF [c]	0.05	15	6.11×10^{-2}	1.22×10^{6}	6.13×10^{3}
	20	60	3.4×10^{-3}	6.81×10^{4}	1.10×10^{5}
MTP [c]	0.05	15	4.62×10^{-2}	0.95×10^{6}	7.89×10^{3}
	20	60	2.9×10^{-3}	5.81×10^{4}	1.26×10^{5}

[a] From [21], [b] From [20] assuming Langmuir kinetics, [c] Results from photocatalytic oxidation of a contaminant mixture [22] where KTR, DCF and MTP were simultaneously treated, [d] From this work. SF is the Scavenging Factor.

3. Materials and Methods

The materials, methods and experimental set-up are reported in previous works in detail [20–22]. Briefly, the experimental set-up was an external four-lamp reactor that consisted of a 1 L borosilicate glass tank provided with magnetic agitation and inlets for oxygen feed and sampling and outlet for gas exiting. The tank was immersed in a pipe box that also contained four black light lamps that emitted radiation between 350 and 410 nm. The lamps were evenly distributed and attached to the pipe.

4. Conclusions

The main conclusions of this work are:

* The Six Flux Model applied to a central lamp reactor predicts the results of the OVRPA for an external four-lamp photoreactor with deviations lower than 10% with catalyst concentration leading to the highest photon absorption rate. This confirms the results from Monte Carlo methods already published. For low catalyst concentrations, SFM overestimates OVRPA values comparing to those from the Monte Carlo method.

* As expected, the predicted LVRPA values show a radial variation for a given value of the axial dimensionless variable being high at the reactor external wall and practically negligible in the central zone of the photoreactor.

* The OVRPA results confirm the positive effect of catalyst concentration. Thus, for low values of catalyst concentration (<0.1 gL^{-1}), the increase in this variable leads to an increase in OVRPA, while at a higher catalyst concentration, OVRPA goes to a plateau value as a consequence of the higher dispersion or scattering due to the increasing presence of catalyst particles.

* Simplified kinetics allow the determination of the intrinsic reaction rate constant and scavenging factor of hydroxyl radicals. These rate constants increase with the decreasing initial concentration of compounds.

* With the kinetic study, the scavenging factor, SF, of the aqueous solution can also be determined. SF increases with the increase in the initial concentration of the contaminant, and the complex structure of the treated compound formed as a result of the high concentration of byproducts. As expected, for compounds treated with photocatalytic oxidation as a mixture doped to the water, SF yields the same value regardless of the compound results.

Supplementary Materials: The following are available online at https://www.mdpi.com/article/10.3390/catal11101190/s1, Figure S1: LVRPA vs. ξ^* from SFM adapted to the external four lamp photoreactor. Variation with dimensional radial position within the reaction space and catalyst concentration. Catalyst concentration, gL^{-1}: ■ 0.5, ▲ 1, ● 1.5, Figure S2. Confirmation of first order kinetics for KTR, DCF and MTP photocatalytic oxidation. Initial concentration of compounds: 20 mgL^{-1}. Symbols: ■ DCF, ▲ MTP, ● KTR. Experimental results from [4]. Figure S3. Assumed first

order kinetics for photocatalytic oxidation of MCPA (experimental results from [5]). Table S1: Values of parameters applied for SFM and dimensions of external lamp photoreactor. Table S2. OVRPA SFM calculated values at different catalyst concentration.

Author Contributions: Conceptualization, F.J.B.; methodology, F.J.B. and J.R.; software, J.R.; validation, F.J.B.; J.R. and J.-F.G.-A.; investigation, F.J.B., J.R. and J.-F.G.-A.; writing—original draft preparation, F.J.B.; writing—review and editing, F.J.B. and J.R.; project administration, F.J.B.; funding acquisition, F.J.B. All authors have read and agreed to the published version of the manuscript.

Funding: This research was funded by Agencia Estatal de Investigación of Spain (PID2019-104429RB-I00/AEI/10.13039/501100011033).

Conflicts of Interest: The authors declare no conflict of interest.

References

1. Sillanpää, M.; Ncibi, M.C.; Matilainen, A. Advanced oxidation processes for the removal of natural organic matter from drinking water sources: A comprehensive review. *J. Environ. Manag.* **2018**, *208*, 56–76. [CrossRef] [PubMed]
2. Deng, Y.; Zhao, R. Advanced Oxidation Processes (AOPs) in Wastewater Treatment. *Curr. Pollut. Rep.* **2015**, *1*, 167–176. [CrossRef]
3. Chatterjee, D.; Dasgupta, S. Visible light induced photocatalytic degradation of organic pollutants. *J. Photochem. Photobiol. C Photochem. Rev.* **2005**, *6*, 186–205. [CrossRef]
4. Beltrán, F.J. *Ozone Reaction Kinetics for Water and Wastewater Systems*; CRC Press: Boca Raton, FL, USA, 2004.
5. Mehrjouei, M.; Muller, S.; Moller, D. A review on photocatalytic ozonation used for the treatment of water and wastewater. *Chem. Eng. J.* **2015**, *263*, 209–219. [CrossRef]
6. Bidga, R.J. Considering Fenton's chemistry for wastewater treatment. *Chem. Eng. Prog.* **1995**, *91*, 62–67.
7. Ribeiro, J.P.; Nunes, M.I. Recent trends and developments in Fenton processes for industrial wastewater treatment—A critical review. *Environ. Res.* **2021**, *197*, 110957. [CrossRef]
8. Mills, A.; Davies, R.H.; Worsley, D. Water purification by semiconductor photocatalysis. *Chem. Soc. Rev.* **1993**, *22*, 417–425. [CrossRef]
9. Schneider, J.; Bahnemann, D.; Ye, J.; Puma, L.G.; Dionysiou, D.D. (Eds.) *Photocatalysis, Vol. 1: Fundamentals and Perspectives*; RSC: London, UK, 2016.
10. Li Puma, G.; Khor, J.N.; Brucato, A. Modelling of an annular photocatalytic reactor for water purification: Oxidation of pesticides. *Environ. Sci. Technol.* **2004**, *38*, 3737–3745. [CrossRef]
11. Cassano, A.E.; Martin, C.A.; Brandi, R.J.; Alfano, O.M. Photoreactor analysis and design: Fundamentals and applications. *Ind. Eng. Chem. Res.* **1995**, *34*, 2155–2201. [CrossRef]
12. Zalazar, C.S.; Romero, R.L.; Martin, C.A.; Cassano, A.E. Photocatalytic intrinsic reaction kinetics I: Mineralization of dichloroacetic acid. *Chem. Eng. Sci.* **2005**, *60*, 5240–5254. [CrossRef]
13. Zazueta, A.L.L.; Destaillats, H.; Li Puma, G. Radiation field modeling and optimization of a compact and modular multi-plate photocatalytic reactor (MPPR) for air/water purification by Monte Carlo method. *Chem. Eng. J.* **2013**, *217*, 475–485. [CrossRef]
14. Alvarado-Rolon, O.; Natividad, R.; Ramirez-Garcia, J.; Orozco-Velazco, J.; Hernandez-Servin, J.A.; Ramirez-Serrano, A. Kinetic modelling of paracetamol degradation by photocatalysis: Incorporating the competition for photons by the organic molecule and the photocatalyst. *J. Photochem. Photobiol. A Chem.* **2021**, *4121*, 113252. [CrossRef]
15. Moreira, J.; Serrano, B.; Ortiz, A.; de Lasa, H. Evaluation of Photon Absorption in an Aqueous TiO_2 Slurry Reactor Using Monte Carlo Simulations and Macroscopic Balance. *Ind. Eng. Chem. Res.* **2010**, *49*, 10524–10534. [CrossRef]
16. Brucato, A.; Cassano, A.E.; Grisafi, F.; Montante, G.; Rizzuti, L.; Vella, G. Estimating radiant fields in flat heterogeneous photoreactors by the six-flux model. *AIChE J.* **2006**, *52*, 3882–3890. [CrossRef]
17. Li Puma, G.; Brucato, A. Dimensionless analysis of slurry photocatalytic reactors using two-flux and six-flux radiation absorption–scattering models. *Cat. Today* **2007**, *122*, 78–90. [CrossRef]
18. Beltrán, F.J.; Aguinaco, A.; García-Araya, J.F.; Oropesa, A. Ozone and photocatalytic processes to remove the antibiotic sulfamethoxazole from water. *Water Res.* **2008**, *42*, 3799–3808. [CrossRef]
19. Mena, E.; Rey, A.; Beltrán, F.J. TiO_2 photocatalytic oxidation of a mixture of emerging contaminants: A kinetic study independent of radiation absorption based on the direct-indirect model. *Chem. Eng. J.* **2018**, *339*, 369–380. [CrossRef]
20. Rivas, J.; Solis, R.R.; Gimeno, O.; Sagasti, J. Photocatalytic elimination of aqueous 2-methyl-4-chlorophenoxyacetic acid in the presence of commercial and nitrogen-doped TiO_2. *Int. J. Environ. Sci. Technol.* **2015**, *12*, 513–526. [CrossRef]
21. Rivas, F.J.; Hidalgo, A.; Solís, R.R.; Tierno, M. Photocatalysis in an external four-lamp reactor: Modelling and validation—dichloroacetic acid photo-oxidation in the presence of TiO_2. *Int. J. Environ. Sci. Technol.* **2019**, *16*, 6705–6716. [CrossRef]
22. Encinas, A.; Rivas, F.J.; Beltrán, F.J.; Oropesa, A. Combination of black-light photocatalysis and ozonation for emerging contaminants degradation in secondary effluents. *Chem. Eng. Technol.* **2013**, *36*, 492–499. [CrossRef]
23. Chong, M.N.; Jin, B.; Chow, C.W.K.; Saint, C. Recent developments in photocatalytic water treatment technology: A review. *Water Res.* **2010**, *44*, 2997–3027. [CrossRef]

24. Liu, B.; Zhao, X.; Terashima, C.; Fujishima, A.; Nakata, K. Thermodynamic and kinetic analysis of heterogeneous photocatalysis for semiconductor systems. *Phys. Chem. Chem. Phys.* **2014**, *16*, 8751. [CrossRef]
25. Malato, S.; Fernandez-Ibañez, P.; Maldonado, M.I.; Blanco, J.; Gernjak, W. Decontamination and disinfection of water by solar photocatalysis: Recent overview and trends. *Catal. Today* **2009**, *147*, 1–59. [CrossRef]
26. Legrini, O.; Oliveros, E.; Braun, A.M. Photochemical processes for water treatment. *Chem. Rev.* **1993**, *93*, 671–698. [CrossRef]
27. Beltrán, F.J.; Rey, A. Free Radical and Direct Ozone Reaction Competition to Remove Priority and Pharmaceutical Water Contaminants with Single and Hydrogen Peroxide Ozonation Systems. *Ozone Sci. Eng.* **2018**, *40*, 251–265. [CrossRef]
28. Beltrán, F.J.; Checa, M.; Rivas, F.J.; García-Araya, J.F. Modeling the Mineralization Kinetics of Visible Led Graphene Oxide/Titania Photocatalytic Ozonation of an Urban Wastewater Containing Pharmaceutical Compounds. *Catalysts* **2020**, *10*, 1256. [CrossRef]
29. Zhai, X.; Chen, Z.; Zhao, S.; Wang, H.; Yang, L. Enhanced ozonation of dichloroacetic acid in aqueous solution using nanometer ZnO powders. *J. Environ. Sci.* **2010**, *22*, 1527–1533. [CrossRef]
30. Benitez, F.J.; Acero, J.L.; Real, F.J.; Roman, S. Oxidation of MCPA and 2,4-D by UV Radiation, Ozone, and the Combinations UV/H_2O_2 and O_3/H_2O_2. *Environ. Sci. Health Part B* **2004**, *39*, 393–409. [CrossRef]
31. Benner, J.; Salhi, E.; Ternes, T.; von Gunten, U. Ozonation of drinking water: Part I. Oxidation kinetics and product formation. *Water Res.* **2008**, *42*, 3003–3012. [CrossRef]
32. Huber, M.M.; Canonica, S.; Park, G.Y.; von Gunten, U. Oxidation of Pharmaceuticals during Ozonation and Advanced Oxidation Processes. *Environ. Sci. Technol.* **2003**, *37*, 1016–1024. [CrossRef]
33. Chen, Y.W.; Hsu, Y.H. Effects of Reaction Temperature on the Photocatalytic Activity of TiO_2 with Pd and Cu Cocatalysts. *Catalysts* **2021**, *11*, 966. [CrossRef]
34. Zertal, A.; Molnár-Gábor, D.; Malouki, M.A.; Sehili, T.; Boule, P. Photocatalytic transformation of 4-chloro-2-methylphenoxyacetic acid (MCPA) on several kinds of TiO2. *Appl. Catal. B Environ.* **2004**, *49*, 83–89. [CrossRef]
35. Rodriguez, R.; Blesa, M.A.; Regazzoni, A.E. Surface Complexation at the TiO2 (anatase)/Aqueous Solution Interface: Chemisorption of Catechol. *J. Colloid Interface Sci.* **1996**, *177*, 122. [CrossRef]
36. Tolosana-Moranchel, A.; Casas, J.A.; Carbajo, J.; Faraldos, M.; Bahamonde, A. Influence of TiO_2 optical parameters in a slurry photocatalytic reactor: Kinetic modelling. *Appl. Catal. B Environ.* **2017**, *200*, 164–173. [CrossRef]